

# JGR Space Physics

## RESEARCH ARTICLE

10.1029/2018JA026251

### Key Points:

- Low-altitude transient ionospheric layers may be explained by a geometric observational effect from localized, not hemispheric, ionization
- A radio occultation of a transient ionospheric layer was obtained with observations of variable proton aurora and penetrating solar wind
- Transient layers observed at Mars, Venus, and Titan are consistent with the presence of solar wind impact ionization at those planets

### Correspondence to:

M. M. J. Crismani,  
matteo.crismani@colorado.edu

### Citation:

Crismani, M. M. J., Deighan, J., Schneider, N. M., Plane, J. M. C., Withers, P., Halekas, J., et al. (2019). Localized ionization hypothesis for transient ionospheric layers. *Journal of Geophysical Research: Space Physics*, 124. <https://doi.org/10.1029/2018JA026251>

Received 9 JAN 2019

Accepted 15 APR 2019

Accepted article online 29 APR 2019

## Localized Ionization Hypothesis for Transient Ionospheric Layers

M. M. J. Crismani<sup>1,2</sup> , J. Deighan<sup>1</sup> , N. M. Schneider<sup>1</sup> , J. M. C. Plane<sup>3</sup> , P. Withers<sup>4</sup> , J. Halekas<sup>5</sup> , M. Chaffin<sup>1</sup> , and S. Jain<sup>1</sup> 

<sup>1</sup>Laboratory for Atmospheric and Space Physics, University of Colorado Boulder, Boulder, CO, USA, <sup>2</sup>NPP/USRA, NASA Goddard Space Flight Center, Planetary Systems Laboratory, Code 693, Greenbelt, MD, USA, <sup>3</sup>School of Chemistry, University of Leeds, Leeds, UK, <sup>4</sup>Center for Space Physics, Boston University, Boston, MA, USA, <sup>5</sup>Department of Physics and Astronomy, University of Iowa, Iowa City, IA, USA

**Abstract** The persistent two-peaked vertical structure of the Martian ionosphere is created by extreme and far ultraviolet radiation whose energies, respectively, determine their ionization altitude. A third low-altitude transient layer (previously referred to as  $M3$  or  $M_m$ ) has been observed by radio occultation techniques and attributed to meteor ablation. However, recent remote sensing and in situ observations disfavor a meteoric origin. Here we propose an alternative hypothesis for these apparent layers associated with impact ionization from penetrating solar wind ions, previously observed as proton aurora. Localized ionization, occurring nonglobally at a given altitude range, breaks the symmetry assumed by the radio occultation technique, and creates electron layers apparently lower in the ionosphere than their true altitude. This may occur when the upstream bow shock is altered by a radial interplanetary magnetic field configuration, which allows the solar wind to penetrate directly into the thermosphere. This localized ionization hypothesis provides an explanation for apparent layers' wide variation in heights and their transient behavior. Moreover, this hypothesis is testable with new observations by the Mars Atmospheric and Volatile Evolution Radio Occultation Science Experiment in future Mars years. This hypothesis has implications for the ionospheres of Venus and Titan, where similar transient layers have been observed.

**Plain Language Summary** The ionosphere of a planet couples the neutral atmosphere to the exosphere and solar wind. Created by solar ionizing radiation, the ionosphere on the dayside of planet is expected to be hemispherically symmetric. When Mars Express discovered transient low-altitude ionospheric layers in 2005, they were initially predicted to be due to meteor ablation. However, recent observations indicate that they are due to a geometric observational effect related to local, not hemispheric, ionization. Observations from three instruments on Mars Atmospheric and Volatile Evolution are used concurrently to understand this phenomenon. These transient layers have been observed at Venus and Titan as well, and this hypothesis indicates novel physics for those ionospheric systems.

### 1. Previous Interpretation of Transient Layers

The Mars Express (MEX) and Mars Global Surveyor (MGS) missions have observed low-altitude transient ionospheric layers (Pätzold et al., 2005; Withers et al., 2008), which form for an unconstrained length of time. While initially presumed to be meteoric in origin, recent observations by the Mars Atmosphere and Volatile Evolution (MAVEN) Imaging Ultraviolet Spectrograph (IUVS) suggest that a meteoric origin is inadequate (Crismani et al., 2017; Peter, 2018). Meteoric ablation is the result of interplanetary dust grains impacting a planetary upper atmosphere at orbital velocities, resulting in the melting and evaporation of the minerals within the grains. These atoms then undergo chemical reactions with the ambient gases that result in the formation of ion layers, such as  $\text{Fe}^+$  and  $\text{Mg}^+$ , which are observed at both Earth and Mars (Grebowsky et al., 2017; Plane, Flynn, et al., 2018). IUVS observations of  $\text{Mg}^+$  densities over the course of more than three Earth years indicates that meteoric ion densities are 2 orders of magnitude smaller than required to explain the observations of MEX and MGS, except in rare meteor showers, such as that from comet Siding Spring (Schneider, Deighan, Stewart, et al., 2015; Crismani et al., 2018).

Transient layers observed by MEX and MGS appear to occur at altitudes ranging from 60 to 120 km, being detached when below the main ionospheric peaks or merged when near these peaks ( $M1$  at 120 km and  $M2$  at 140 km). A recent comprehensive analysis by Peter (2018) looked at the occurrence of merged

layers in the MEx data set and compared them to a modern 1-D ion-neutral chemical model. They found considerable difficulty in identifying processes capable of depositing sufficient ionizing energy at altitudes where transient layers are found in the absence of a meteoric origin. Ionization due to penetration of solar energetic particles and soft X-ray fluxes has also been proposed; however, existing data sets do not exhibit a clear correlation with detached layers nor is it clear that these sources would provide sufficient energetic penetration below 100 km to generate separated layers of electron concentration.

The topside ionosphere of Mars (>170 km) exhibits strong variability; however, this is unlikely to affect the peak ionospheric densities in the main layer (*M2*). At the location of the main peak, the ionosphere is coupled to the neutral atmosphere and chemical lifetimes are short compared to transport effects (Mendillo, Narvaez, Vogt, Mayyasi, Forbes, et al., 2017). Therefore, topside variability observed both by in situ data and remote sensing, such as in Fowler et al. (2018) or Kopf et al. (2008), respectively, and reviewed in detail by Withers (2009), occurs in a region where chemical processes compete with plasma dynamics, that is, Kelvin-Helmholtz instabilities driving large amplitude waves. In the lower ionosphere, ion densities are controlled by ionization of the neutral atmosphere and variations of that neutral background, that is, CO<sub>2</sub> variability dominated by wave-2 nonmigrating tides (Mendillo, Narvaez, Vogt, Mayyasi, Mahaffy, et al., 2017).

Radio occultation observations occur in geometries where the Earth becomes occulted by the planet's atmosphere as the spacecraft moves through its orbit. Various programmatic issues and aspects of the occultation technique constrain the frequency of observations, such that observations by MEx and MGS occur between Mars years 24 and 27, and between solar zenith angles of 50–110°. The MEx analysis found detached layers in 10/120 profiles (Pätzold et al., 2005), compared to the MGS data set that contained 71/5,600 profiles (likely due in part to the difference in radio occultation data qualities; Withers et al., 2008), or to the merged layer analysis that contained 117/266 profiles (Peter, 2018). A careful study of the physical characteristics of detached layers found in the MGS data set was undertaken (Withers et al., 2008), which explored correlations between observed characteristics of these layers, the ionosphere, and meteor streams. Withers et al. (2008) noted that the range of the width of these layers was large, 1–27 km, and correlated with their heights. To observe transient layers that are merged with the lower *M1* layer, the main peaks must be fit by a Chapman model and subtracted (Peter, 2018). The mean peak electron concentrations inferred in those merged observations were  $0.8 \times 10^5$  electrons/cm<sup>3</sup>, in contrast to the detached layers whose mean peak concentration is  $1.3 \times 10^5$  electrons/cm<sup>3</sup>. Moreover, the occurrence rate of a detached layer appears correlated with altitude, showing only one observed below 80 km, 25 between 80 and 90 km, and 40 between 90 and 100 km (Withers et al., 2008).

Observations of transient ionospheric layers occur more frequently in Martian southern hemisphere summer (49 of the 71 MGS observed layers), but this has not been explained (Withers et al., 2008). This season is typically associated with enhanced global dust activity; however, the work of Withers et al. (2008) shows that transient layers did not correlate with dust opacity. It should also be noted that while the observations of MGS occurred during southern summer these occultations were measured in the northern hemisphere. Recent analysis by Gupta and Upadhyaya (2019) suggests that the occurrence rate of transient layers is increased by those sources which enhance the lower primary layer (*M1* at 115 km) and is not associated with expected meteor showers or dust storms.

On 10 October 2017, the MAVEN Radio Occultation Science Experiment (ROSE; Withers et al., 2018) observed a transient layer near 60 km, whose peak electron concentration was  $2.5 \times 10^5$  electrons/cm<sup>3</sup> (Figure 1). Transient layers were not observed in any previous observations reported in the ROSE first results paper of Withers et al. (2018). This layer is among the lowest altitude reported in the literature, with a concentration at the peak slightly above the average for this type of event. The ROSE experiment makes radio occultations whenever programmatically feasible; however, there are no occultations in the orbits directly before or after this time period. Observations of meteoric ions from this time period were obtained by IUVS, and are consistent with the production of no significant additional Mg<sup>+</sup> above the background average (Figure 2).

## 2. Spatial Asymmetry in Radio Occultations

Radio occultation measurements are made by determining the relative refraction of the radio signal broadcast by the spacecraft as observed from Earth. This results in a frequency residual that is first inverted to

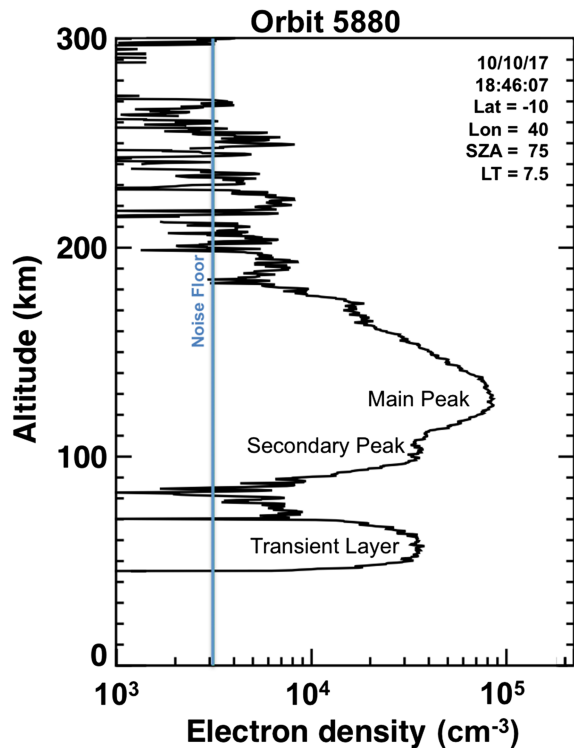


**Figure 1.** A Radio Occultation Science Experiment (ROSE) profile from 10 October 2017, which features a transient ionospheric layer at a tangent altitude of 60 km, whose peak electron density is  $2.5 \times 10^4 \text{ e}^-/\text{cm}^3$ . This observation occurs on the dawn terminator of the planet near the equator. This occultation is conducted after periapse of orbit 5880, while MAVEN is on the outbound segment moving toward apoapse. The vertical blue line denotes the noise floor, and a description of the data processing is found in Withers et al. (2018).

produce a line of sight column of electrons, and subsequently a concentration of electrons at the tangent point. A critical assumption of the data processing techniques used for radio occultation measurements is spherical symmetry. Retrievals through the refractive medium, the ionosphere and neutral atmosphere in this case, occur along one dimension, and therefore, other dimensions remain unconstrained. We describe here the effect of spatial asymmetry on radio occultation techniques and how this is a probable explanation for observations of apparent low-altitude ionospheric layers on the dayside of a planetary atmosphere.

Spatial symmetry is expected on the dayside of Mars, as the primary ionization source is uniform insolation by ultraviolet radiation and ion lifetimes are short compared to transport time scales. On the nightside of Mars, the ionosphere is sourced by day-night transport and electron precipitation, so the assumption of spatial symmetry can be relaxed. This has been addressed in Withers et al. (2012), where they showed that there is a relevant length scale over which uniformity must occur in order for spherical symmetry to be a valid assumption, and for a radio occultation retrieval to be considered representative of the local conditions at the tangent point. For a neutral scale height of 10 km, they determine this length scale is on the order of 250 km. Furthermore, they address the repercussions of spatial asymmetries on the retrieval process, and conclude the following points (adapted from Withers et al., 2012):

1. If a localized region of high-density plasma some horizontal distance away from the occultation point, [...] then the altitude of the layer in the derived density profile is at or below the true altitude [...].
2. The density of the plasma in the derived layer underestimates the true density of this localized region of high-density plasma.

Here we propose that spatial asymmetry affects a retrieved electron profile by artificially lowering the perceived altitude (Figure 3). To demonstrate this effect, we created a simple model of a spherically symmetric single-peaked ionosphere, and added a region of enhanced ionization. To recreate

a layer at 60 km with similar characteristics as those observed by ROSE (Figure 1), we created a layer whose angular width about the planet is  $4^\circ$ , offset from the tangent point (defined as  $0^\circ$  zenith angle) by  $11^\circ$ . We chose a true altitude of 125 km and peak concentration twice that of the main ionospheric peak, although with a separate perturbed scale height. The perceived magnitude of this enhancement at the tangent point is less than the true enhancement, and is sensitive to its angular width and offset. As the perturbation is lowered (say to 100 km), this decreases the angular width (from  $11^\circ$  to  $8^\circ$ ) necessary to locate the transient layer at the observed tangent point. We also compared this model with previous observations, such as those from Withers et al. (2008), and found that multiple regions of local ionization away from the tangent point readily formed double-peaked structures.

### 3. Hypothesis: Solar Wind Impact as a Local Ionization Source

Mars exhibits three different types of aurora: discrete aurora was first detected by Mars Express (Bertaux et al., 2005), followed by the discovery of two new types by the MAVEN mission. MAVEN was able to observe diffuse aurora, where solar energetic particles impact the upper atmosphere, producing auroral emissions at all longitudes on the nightside (Schneider, Deighan, Jain, et al., 2015; Schneider et al., 2018). While these two auroral phenomena are associated with solar energetic particles, a third type of aurora was also discovered with a different production mechanism. Proton aurora was originally discovered at Earth (Eather, 1967; Kallio & Barabash, 2001), and this process occurs similarly at Mars (Deighan et al., 2018; Ritter et al., 2018). Proton aurora occur when solar wind protons charge exchange with the planet's neutral hydrogen corona, creating energetic neutral atoms that are capable of penetrating the magnetospheric boundary layer, or foreshock, and delivering energy to the upper atmosphere (Deighan et al., 2018; Ritter et al., 2018).

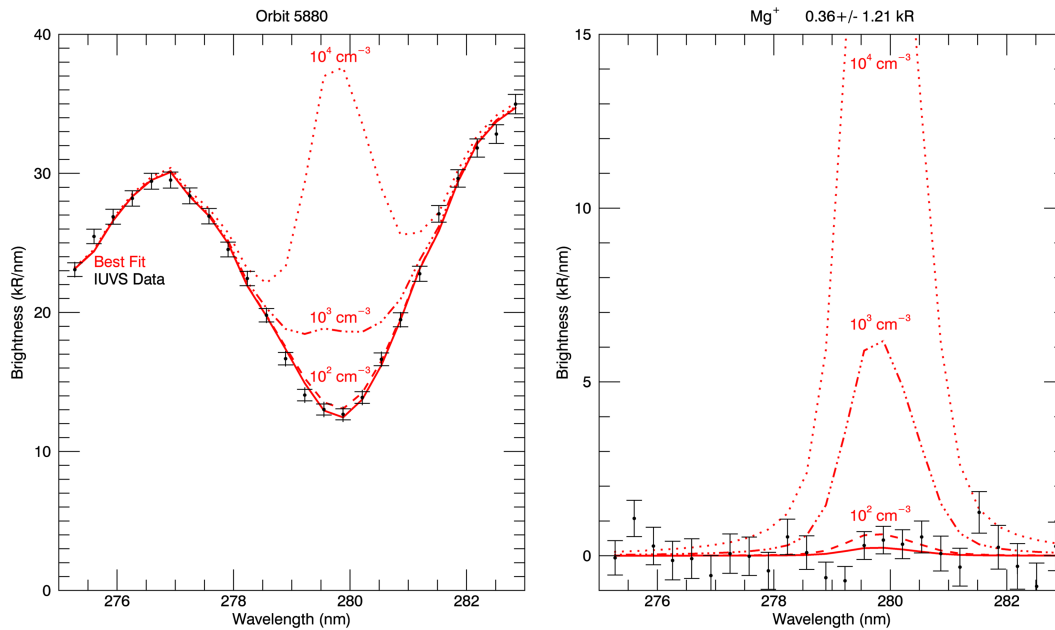


**Figure 2.** (left) Imaging Ultraviolet Spectrograph (IUVS) observed spectra (black) from orbit 5880 (10/10/17 16:14 UTC) at 60 km, with the best fit (solid red) composed of the combination of known emissions, such as scattered solar continuum,  $Mg^+$ , and ambient gases. Broken lines show varying expected  $Mg^+$  emission as local ion concentrations are artificially enhanced. (right) The difference between the observed spectra and the best fit gives the residual (black) which is compared to  $Mg^+$  emission profiles of artificial concentrations. The solid red indicates the best fit  $Mg^+$ , and is consistent with a nondetection of enhanced metallic ions during this time period.

Proton aurora are expected to be enhanced during Martian southern hemisphere summer ( $L_s \sim 300$ ), as the hydrogen corona is seasonally inflated (Chaffin et al., 2014; Clarke et al., 2014), which leads to enhanced charge exchange upstream from Mars (Deighan et al., 2018; Halekas et al., 2017). Energetic neutrals created in the solar wind maintain the solar wind velocity ( $\sim 300\text{--}600$  km/s), travel unimpeded by magnetic and electric fields, and impact the atmosphere. These neutrals transfer energy and momentum, interact chemically through electron stripping and charge exchange, and ionize the neutral atmosphere (Fang et al., 2013; Gerard et al., 2018).

Ion chemistry at Mars is strongly dependent on the presence of  $CO_2$  and the solar ionizing flux, which results in the dominant ion  $O_2^+$ , formed through charge exchange of O atoms with  $CO_2^+$ . The lifetime of electrons is therefore essentially governed by electron dissociative recombination:

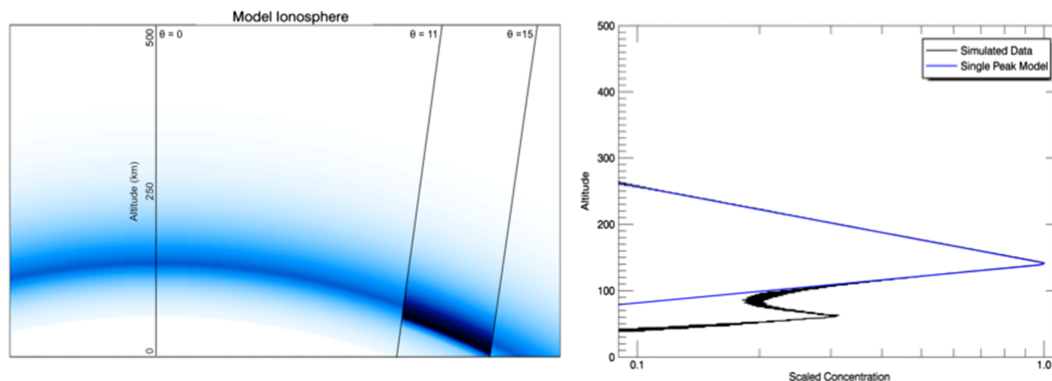


**Figure 3.** A two-dimensional cross section of Mars' modeled ionosphere from which we construct the simulated radio occultation profile. (left) The atmosphere of the planet is shown curving about its limb, with the surface of the planet shown at 0-km altitude and increasing vertically. The geometric parameters of the enhancement are indicated, with increasing angle away from the observed tangent point. (right) The ionosphere from left is integrated along the line of sight, and inverted with an Abel Transform to simulate the radio occultation data processing technique. The unperturbed ionosphere is represented by an oversimplified single peak model (blue) and scaled to unity to emphasize the perturbed enhancement (black) of 30% that appears at low altitude.



where the rate coefficient  $k_1$  is  $5 \times 10^{-7} \text{ cm}^3/\text{s}$  (Bones et al., 2015). In steady state, the rate of production of electrons ( $P$ ) is equal to their removal.

$$k_1[\text{e}^-][\text{O}_2^+] = k_1[\text{e}^-]^2 \quad (2)$$

with charge neutrality maintained:

$$[\text{O}_2^+] = [\text{e}^-] \quad (3)$$

Hence,  $310 \text{ cm}^{-3}/\text{s}$  for a layer with  $[\text{e}^-] = 2.5 \times 10^4 \text{ electrons/cm}^3$ , which matches the concentration at the apparent tangent point in Figure 1. This rate underestimates the true ionization rate if we do not assume that spatial symmetry is appropriate. For such a layer (described above) at 125 km whose true electron concentration is  $1.8 \times 10^5 \text{ electrons/cm}^3$ , the ionization rate must then be  $16,200 \text{ cm}^{-3}/\text{s}$ . As stated above, this rate is dependent on the precise geometry but not on the production process, and plausible ionization processes must be capable of producing this rate. These considerations are under the assumption of steady state, which is valid for time scales larger than the order of tens of minutes.

#### 4. Concurrent Observations Support a Local Ionization Hypothesis

For global proton events (such as those reported in Deighan et al. (2018)), ionization that occurs uniformly near the  $M1$  or  $M2$  peaks is indistinguishable from nominal enhancements in the solar ionizing flux. For ionization that appears below the main peaks, it is not immediately obvious whether this is due to spatial or temporal variations. Ionization of the main layers that occurred after the radio occultation tangent altitude had passed below them would appear as increased ionization at low altitude. However, solar temporal perturbations of the ionosphere are not rapid compared to the duration of an occultation, where flares increase ionization on the order of minutes and the segment of an occultation that occurs below the peaks are on the order of tens of seconds (Fallows et al., 2015; Mendillo & Evans, 1974). Therefore, solar flares cannot explain the low-altitude transient layers.

The MAVEN mission can test the local ionization hypothesis with three sets of observations: IUVS Hydrogen Ly $\alpha$  limb profiles, Solar Wind Ion Analyzer (SWIA) periapse energy spectrum, and ROSE electron density profiles. Using the SWIA energy spectrum, measured in situ at the spacecraft as it moves through periapse, we can connect the observations of Ly $\alpha$  on the limb with their expected source, noting that both appear spatially varying (Figures 4 and 5). While spatial variation is the strongest evidence for local ionization, the remote sensing observations of IUVS and in situ observations of SWIA are taken at separate locations (as far as 1,000 km away), and this evidence is strongly based on a temporal correlation in observations. It is worth noting that MAVEN carries a solar energetic particle detector, which observes energetic ions with energies of 20 keV–6 MeV (Larson et al., 2015). However, during this time period there was no signature of a CME, solar event, or the presence of solar energetic particle precipitation outside of the typical as determined with the methods of Lee et al. (2017).

Figure 4 shows IUVS observations of Hydrogen Ly $\alpha$  emission at 121 nm during MAVEN's periapse segment. These pseudo-images are constructed by scanning the  $10.6^\circ$  airglow slit tangent to the planet's limb perpendicular to the direction of motion with an internal scan mirror. The periapse segment takes about 45 min and consists of 12 scans over horizontal distance of 6,000 km parallel to MAVEN's orbit. The periapse segment of orbits 5879 and 5800 occurred near 10 October 2017 11:48 and 16:14 UTC, a local time near 15:30 hr, centered near latitude 20 and longitudes 250 and 180, respectively. An orbit without proton aurora is shown (top, orbit 5879), where the vertical variation in Ly $\alpha$  does not change rapidly due to the large scale height of atomic hydrogen ( $>500 \text{ km}$ ). The Ly $\alpha$  signal is greatly attenuated below 120 km due to absorption by  $\text{CO}_2$  (Gerard et al., 2018). Orbit 5879 and orbit 5880 occur 5.5 and 1 hr before the radio occultation of Figure 1, although the periapse scans occur near dusk and ROSE's observation is near dawn. In the bottom panel of Figure 4 (orbit 5880) there is an enhancement in Ly $\alpha$ , although not in every scan. This lack of spatial symmetry suggests either that the time scale of the proton aurora process is on the order of the scan time ( $\sim 4 \text{ min}$ ), or that there is spatial asymmetry on the order of the scan-to-scan distance (100 km). Note

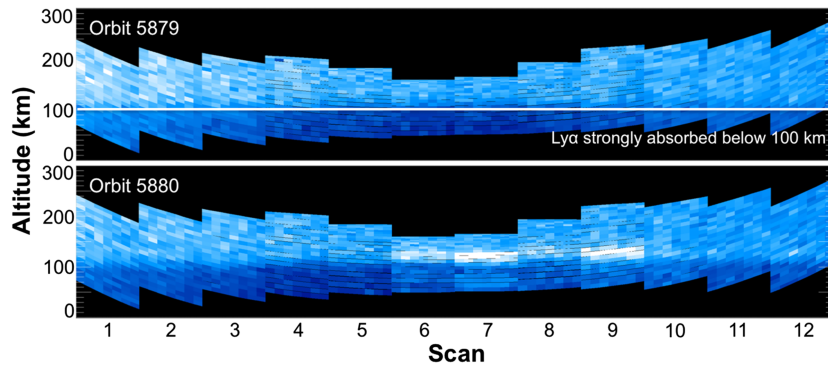


**Figure 4.** An Imaging Ultraviolet Spectrograph (IUVS) periaipse observations of Hydrogen Ly $\alpha$  emission, where the 10.6° airglow slit is moved with a scan mirror to image the limb. The periaipse segment takes about 45 min and consists of 12 scans over horizontal distance of 6,000 km along track. (top) An observation from 5.5 hr before the ROSE occultation of Figure 1 shows a typical periaipse in the absence of proton aurora, taken in orbit 5879 at October 10 2017 11:48 UTC. Hydrogen Ly $\alpha$  emission is strongly absorbed by CO $_2$  below 120 km, which leads to relative dimming. (bottom) Periaipse from an hour before the ROSE occultation of Figure 1, where enhanced Ly $\alpha$  emission is due to impact ionization at altitudes near 120 km, taken in orbit 5880 at October 10 2017 16:14 UTC. The brightening below 120 km seen in scan 7 (compared to the previous orbit) indicates that this emission is coming from the foreground, not the tangent point.

that this spatial variation is smaller than the required 250-km uniformity required for radio occultation retrieval of the electron density profile (Withers et al., 2012), as discussed in the previous section.

Observations of Ly $\alpha$  from IUVS are corroborated by detections of solar wind particles deep in the Martian thermosphere during this time period. The MAVEN SWIA measures ions with energies of 5–25 keV, both in the upstream solar wind and within the Martian magnetosphere, dependent on MAVEN’s orbit (Halekas et al., 2015). Figure 5 shows a pair of time series energy spectra obtained by the SWIA instrument across periaipse passes on two adjacent orbits. The data from orbit 5879 (top) exemplifies the typical exclusion of solar wind particles from the Martian thermosphere. However, in orbit 5880 (bottom) a very unusual

phenomenon is observed, where penetrating solar wind particles appear as a relatively continuous distribution across all altitudes. This suggests direct access for these solar wind particles into the thermosphere. There are three bands of energy seen in the SWIA observations, the lower two being consistent with solar wind H $^+$  and He $^{++}$ , but the highest-energy band is unusual. It may be that pickup H $^+$  or O $^+$  is able to penetrate to these altitudes, although we cannot confirm this as SWIA is not capable of unambiguously determining ion composition and the appropriate complementary instrument (STATIC) was not measuring those energies at periaipse. The lack of spatial symmetry throughout periaipse suggests that the variability of penetrating solar wind is on the order of the enhancement near 16:32 UTC (~2 min), and that the relevant spatial scales are ~500 km.

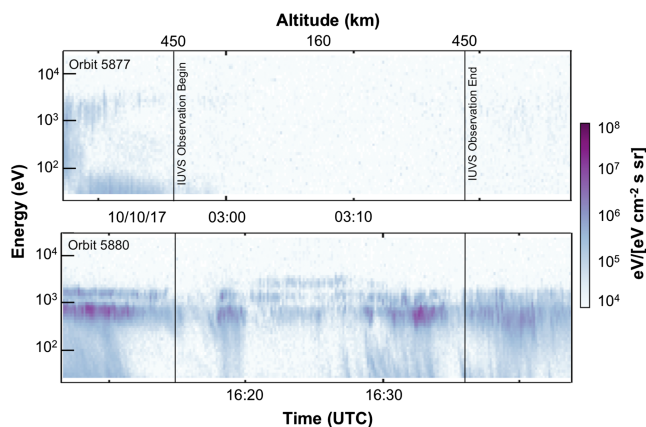


**Figure 5.** A Solar Wind Ion Analyzer (SWIA) energy spectrum is constructed as MAVEN moves through its periaipse segment, with time and altitude on the horizontal axis (see text for details). Periaipse occurs at 160 km, and IUVS observations begin and end at 450 km. (top) A nominal periaipse that shows negligible energetic ion flux above tens of eV across periaipse. (bottom) In contrast, orbit 5880 shows much larger fluxes of particles at solar wind energies of ~1 keV, extending throughout periaipse. Note two bands of energetic ions that appear throughout this orbit, and a third band that appears between 16:20 and 16:30. The spatial distribution of these particles is not homogenous, given the lack of a uniform color or color gradient with altitude, indicating spatial/temporal nonuniformities throughout periaipse.

The Martian bow shock under normal conditions is a strong high Mach number shock with a sharp increase of density and magnetic field and a decrease in flow velocity. The bow shock is followed by a magnetosheath in which the solar wind flow is further decelerated and deflected around Mars. However, during times when the interplanetary magnetic field (IMF) is at or near radial, the structure of the bow shock can change dramatically, becoming fragmented and unsteady. This more complex structure, typical of quasi-parallel shock geometries, is likely due in large part to ion-ion instabilities that steepen and become nonlinear (Schwartz & Burgess, 1991; Thomsen et al., 1990). Such phenomena have been observed by MAVEN’s SWIA and are discussed at length in Halekas et al. (2017). At such times, solar wind ions may at least transiently

penetrate to much lower altitudes than typical. Similar cases of “disappearing magnetospheres” have also been observed at Venus (Zhang et al., 2009). Due to the elliptical nature of MAVEN’s orbit, it is only rarely possible for SWIA to observe at periape on the dayside of Mars while also sampling the solar wind at apoapse. Therefore, this potential explanation for the SWIA observations comes from an understanding of similar previous conditions, and cannot be confirmed by concurrent observations of the solar wind for the event described herein.

This observation is unique in the MAVEN data set because of the requirement that three concurrent observations be made under specific observing conditions. IUVS observations of proton aurora occur in about 20% of dayside observations; however, spatially asymmetric observations are very rare (12/5,000, or 2% of dayside observations). The frequencies of transient layers in radio occultations from other spacecraft such as MEX and MGS are observed to be on the order of 10–40%. ROSE observations began in July 2016, and have not yet determined such an occurrence rate. Future work will investigate the SWIA data in detail to characterize the frequency of solar wind penetration as there are likely other events of various penetration intensities. The next possible time periods where coordinated observations of this type are possible are March to May and August to November of 2019.

The inferred ionization rates from the IUVS and SWIA data shown herein are not immediately sufficient to explain the observed ion layer and further modeling will be necessary to test this hypothesis. The flux of hydrogen ENAs required to produce the observed excess Ly $\alpha$  brightness of 1–2 kR would only produce a peak ionization rate of  $\sim 100$  cm $^{-3}$ /s, which is by itself insufficient to explain the ROSE observation. However, unlike typical Martian proton aurora, our hypothesis predicts that these ENAs are not produced by charge exchange with the neutral hydrogen corona in the upstream solar wind, but rather originate from solar wind protons directly charge exchanging with the Martian thermosphere. Therefore, the ratio of protons to ENAs should be very high for this type of event. This is supported by the mean solar wind energy flux observed by SWIA, which suggests an ionization rate of 6,400 cm $^{-3}$ /s near the normal dayglow peak at 140 km.

It should be noted that these estimates do not take into account the true altitude of the deposition and the line of sight Ly $\alpha$  absorption that are necessarily occurring, both of which require self-consistent modeling (Gerard et al., 2018). Further modeling would require the detailed consideration of integrated energy flux of the three species and their ionization cross sections which informs the true penetration depths and relevant deposition scale heights. Since these calculations are nontrivial, we consider that detailed modeling of this type is outside the scope of this work, as it will be necessary to extend such modeling efforts to Venus and Titan’s transient layers. A discussion of the inferred ionization uncertainties associated with the true penetration depth and physical location of penetrating particles will be strongly model dependent, and the above rates should be considered as an order of magnitude result. Therefore, these indirect observations of ionization and their calculated rates are not independent validation of this hypothesis. Instead, the observed spatial variations in those observations are the strongest evidence that radio occultations are not viewing a spatially symmetric dayside ionosphere, as has previously been assumed.

## 5. Implications for Martian Atmospheric Evolution, Titan, and Venus

A localized ionization hypothesis provides a solution to a number of unexplained characteristics of transient ionospheric layers. Their transient nature is explained by the changing solar wind conditions, whose time scale can be quite short (even on the order of hours). The wide variation in transient layer widths is related to geometric effects, which also explains the increasing occurrence frequency with increasing altitude. Warming in the lower atmosphere should inflate the H corona (Chaffin et al., 2017; Heavens et al., 2018; Jakosky et al., 2017); however, this should symmetrically affect proton aurora by overall enhancement in penetrating energetic neutral atoms. Therefore, this hypothesis does not alone explain the correlation of transient layer occurrence with Martian southern summer.

Transient ionospheric layers have been observed at Titan (Kliore et al., 2008) and Venus (Pätzold et al., 2009), and their origin is likely due to localized ionization not meteor ablation, as currently understood. This is indirect evidence that supports the proposition of Deighan et al. (2018) that proton aurora should be a common phenomenon for planets with extended neutral coronas, which are able to extend past the planet’s bow shock. As they note, these conditions occur at Venus (Gombosi et al., 1980), and when Titan

is outside of Saturn's magnetosphere (Bertucci et al., 2015), as well as at close in exoplanets such as HD 209458b (Kislyakova et al., 2014).

Titan's low-altitude transient ionospheric layers demonstrated enhancements between 0.5 and 1 times the main ionospheric peak concentrations, at altitudes originally assumed to be consistent with a meteoric origin (500 km; Kliore et al., 2008). However, subsequent work has demonstrated that a majority of meteors do not ablate in Titan's atmosphere, and the contribution to the ionosphere is expected to be small (Frankland et al., 2016). Moreover, recently analysis of Royer et al. (2018) indicates enhanced airglow emission when Titan is outside of Saturn's magnetopause, concurrent with observations of an unusual electron burst. Therefore, it is likely that the assumption of spherically symmetry is also inappropriate for Titan, whose ionosphere may be more complex than currently understood.

Some transient ionospheric layers observed at Venus (Pätzold et al., 2009) and Mars (Withers et al., 2008) are unique as they show more than one layer in an occultation. Meteor ablation models, such as CABMOD (Carrillo-Sánchez et al., 2016; Plane, Carrillo-Sanchez, et al., 2018), do not readily explain such enhancements, as the difference in the ablation heights require atypical values for meteor velocities and vertical mixing rates are expected to smooth out such profiles that observation of the separation appears extremely coincidental. However, the localized ionization hypothesis would predict such an occurrence when several regions of ionization are distributed in the foreground/background of the observation.

The localized ionization hypothesis suggests a potentially nonnegligible source of ionization has hitherto not been considered. Solar wind impact ionization is likely to occur consistently at a low level (Ritter et al., 2017), interspersed with more significant events. As the radio occultation method reduces the true local ionization when retrieving it at the tangent point, the ionization of these patches are comparable to the UV ionizing flux which creates the main peaks. While this is unlikely to be a dominant loss process (for a full discussion see Jakosky et al. (2018)), it may be important to consider when assessing overall atmospheric evolution from planets with extended neutral coronas. If this hypothesis is validated by future observations by MAVEN, attention should be paid to the literature that has referenced these layers, and reevaluation of their results and conclusions may be necessary.

## 6. Conclusions

Martian low-altitude transient ionospheric layers have presented a mystery since their meteoric origin was challenged by MAVEN observations of meteoric ions (Crismani et al., 2017; Grebowsky et al., 2017). Transient layers appeared to occur at altitudes below the main ionospheric peak at 120 km to as low as 60 km, deep within the neutral atmosphere. More perplexing, transient ionospheric layers were observed more frequently in Martian southern hemisphere summer and this correlation is still not understood.

Planetary radio occultations are made by determining the relative refraction of the spacecraft's radio signal in geometries where the Earth becomes occulted by the planet's atmosphere and ionosphere. The process of retrieving electron concentrations from such observations assumes hemispheric symmetry, which has previously been expected on the dayside of unmagnetized planets. At Mars, EUV is the primary ionization source, and near the main ionospheric layer ( $M2$  at 120 km) ion lifetimes are short compared to transport time scales. Ion chemistry at these altitudes is strongly dependent on the presence of  $\text{CO}_2$ , which forms the dominant ion  $\text{O}_2^+$  through charge exchange. While the topside ionosphere of Mars (>170 km) exhibits variability due to various dynamical plasma processes, the main layer is coupled to the neutral atmosphere and its variability is the result of changes in the neutral atmosphere.

This work proposes that ionospheric spatial asymmetry affect a retrieved electron profile from radio occultations by artificially lowering the perceived altitude. We posit that this geometric effect explains the variation in altitude of observed transient layers, as well as their nonuniform distribution in altitude. The recent discovery of proton aurora (Deighan et al., 2018) presents a hitherto unconsidered source of energy and ionization. Typically, proton aurora events are global and the resulting ionization occurs uniformly; however, a small fraction of events show spatial asymmetry.

Serendipitous observations by three MAVEN instruments support, but do not yet prove, a localized ionization hypothesis: ROSE electron density profiles, IUVS Hydrogen Ly $\alpha$  vertical profiles, and SWIA energy spectra. This set of observations is unique in the MAVEN data set due to the recent

commissioning of the ROSE instrument, and the requirement of specific observing conditions. Although the Martian bow shock typically exhibits a strong shock with a sharp dense boundary, there exist conditions when the IMF is at or near radial where the bow shock becomes fragmented and unsteady. Such conditions were likely met on 10 October 2017, when ROSE observed a transient layer near 60 km, IUVS observed Hydrogen Ly $\alpha$  emission from proton aurora, and SWIA observed solar wind particles in the Martian thermosphere. One cannot say with certainty whether the IMF was radial at this time as SWIA was not in the upstream solar wind; however, these IMF configurations have previously been reported (Halekas et al., 2017).

Impact ionization is therefore a plausible hypothesis for the origin of transient layers, although further modeling is required. There exists a discrepancy in the inferred ionization rates from the IUVS and SWIA observations, which must be resolved self-consistently. The true penetration depths and relevant deposition scale heights of these solar wind particles requires consideration of their integrated energy flux and their ionization cross sections. Moreover, IUVS observations underestimate the true ionization rate due to line-of-sight absorption of Ly $\alpha$ , which must independently be determined.

Ionospheric electron densities above crustal magnetic fields are enhanced above 200 km, an effect observed in situ and with remote sensing (Andersson et al., 2015; Flynn et al., 2017; Withers et al., 2018). Peter (2018) infers the presence of transient layers to be uncorrelated with the crustal magnetic field regions as there are an abundance of observations of such layers in the Northern Hemisphere and away from crustal regions. If crustal magnetic fields can influence the spatial distribution of ions near the main peak, where chemical lifetimes are short, there may be regions of enhanced ionization which appear as transient layers in radio occultation. Without concurrent radio occultation and SWIA observations of penetrating particles, there is no way to distinguish between magnetic control and impact ionization. There were no reported transient layers during the observations of Withers et al. (2018), which includes five occultations over strong fields in August–October 2016. Future observations over the southern hemisphere may be able to resolve the importance of magnetic control near the main peak.

Future coordinated observations by ROSE, IUVS, and SWIA will be able to verify the relationship between spatially asymmetric solar wind penetration and transient layers in radio occultation. However, existing data sets may also be investigated to inform modeling efforts and determine the relationship between SWIA penetrating particles and IUVS spatially asymmetric proton aurora. These aurorae have been observed in ~2% of dayside observations, which indicates that there may exist a handful of SWIA observations out of the several thousand that demonstrate unusual penetration signatures. Without a systematic investigation of SWIA data, we cannot say how unusual or energetic the event described herein, as would be necessary for incorporation in future modeling and atmospheric evolution discussions.

#### Acknowledgments

M.C. thanks E. Royer for enlightening discussions about Titan's ionosphere and two anonymous reviewers for their suggestions. M.C. was supported in part by the NASA Postdoctoral Program at the NASA Goddard Space Flight Center, administered by Universities Space Research Association (USRA) under contract with NASA. NASA supports the MAVEN mission through the Mars Scout program. J.M.C.P. was supported by the European Research Council (project 291332 - CODITA). All data used herein are available on the Atmospheres node of the NASA Planetary Data System. The authors declare no competing financial interests.

#### References

- Andersson, L., Ergun, R. E., Delory, G. T., Eriksson, A., Westfall, J., Reed, H., et al. (2015). The Langmuir probe and waves (LPW) instrument for MAVEN. *Space Science Reviews*, 195(1-4), 173–198. <https://doi.org/10.1007/s11214-015-0194-3>
- Bertaux, J.-L., Leblanc, F., Witasse, O., Quémérais, E., Lilensten, J., Stern, S. A., et al. (2005). Discovery of an aurora on Mars. *Nature*, 435(7043), 790–794. <https://doi.org/10.1038/nature03603>
- Bones, D. L., Plane, J. M. C., & Feng, W. (2015). Dissociative recombination of FeO<sup>+</sup> with electrons: Implications for plasma layers in the ionosphere. *The Journal of Physical Chemistry A*, 120(9), 1,369–1,376.
- Bertucci, C., Hamilton, D. C., Kurth, W. S., Hospodarsky, G., Mitchell, D., Sergis, N., et al. (2015). Titan's interaction with the supersonic solar wind. *Geophysical Research Letters*, 42, 193–200. <https://doi.org/10.1002/2014GL062106>
- Carrillo-Sánchez, J. D., Nesvorný, D., Pokorný, P., Janches, D., & Plane, J. M. C. (2016). Sources of cosmic dust in the Earth's atmosphere. *Geophysical Research Letters*, 43, 11,979–11,986. <https://doi.org/10.1002/2016GL071697>
- Chaffin, M. S., Deighan, J., Schneider, N. M., & Stewart, A. I. F. (2017). Elevated atmospheric escape of atomic hydrogen from Mars induced by high-altitude water. *Nature Geoscience*, 10(3), 174–178. <https://doi.org/10.1038/ngeo2887>
- Chaffin, M. S., Chaufray, J.-Y., Stewart, I., Montmessin, F., Schneider, N. M., & Bertaux, J.-L. (2014). Unexpected variability of Martian hydrogen escape. *Geophysical Research Letters*, 41, 314–320. <https://doi.org/10.1002/2013GL058578>
- Clarke, J. T., Bertaux, J.-L., Chaufray, J.-Y., Gladstone, G. R., Quémérais, E., Wilson, J. K., & Bhattacharyya, D. (2014). A rapid decrease of the hydrogen corona of Mars. *Geophysical Research Letters*, 41, 8013–8020. <https://doi.org/10.1002/2014GL061803>
- Crismani, M. M. J., Schneider, N. M., Evans, J. S., Plane, J. M. C., Carrillo-Sánchez, J. D., Jain, S., et al. (2018). Impact of comet siding spring's meteors on the atmosphere and ionosphere of Mars. *Journal of Geophysical Research: Planets*, 123, 2613–2627. <https://doi.org/10.1029/2018JE005750>
- Crismani, M. M. J., Schneider, N. M., Plane, J. M. C., Evans, J. S., Jain, S. K., Chaffin, M. S., et al. (2017). Detection of a persistent meteoric metal layer in the Martian atmosphere. *Nature Geoscience*, 10(6), 401–404. <https://doi.org/10.1038/ngeo2958>
- Deighan, J., Jain, S. K., Chaffin, M. S., Fang, X., Halekas, J. S., Clarke, J. T., et al. (2018). Discovery of a proton aurora at Mars. *Nature Astronomy*, 2, 802–807.

- Eather, R. H. (1967). Auroral proton precipitation and hydrogen emissions. *Reviews of Geophysics*, 5(3), 207–285. <https://doi.org/10.1029/RG005i003p00207>
- Fallows, K., Withers, P., & Gonzalez, G. (2015). Response of the Mars ionosphere to solar flares: Analysis of MGS radio occultation data. *Journal of Geophysical Research: Space Physics*, 120, 9805–9825. <https://doi.org/10.1002/2015JA021108>
- Fang, X., Lummerzheim, D., & Jackman, C. H. (2013). Proton impact ionization and a fast calculation method. *Journal of Geophysical Research: Space Physics*, 118, 5369–5378. <https://doi.org/10.1002/jgra.50484>
- Flynn, C. L., Vogt, M. F., Withers, P., Andersson, L., England, S., & Liu, G. (2017). MAVEN observations of the effects of crustal magnetic fields on electron density and temperature in the Martian dayside ionosphere. *Geophysical Research Letters*, 44, 10,812–10,821. <https://doi.org/10.1002/2017GL075367>
- Fowler, C. M., Andersson, L., Ergun, R. E., Harada, Y., Hara, T., Collinson, G., et al. (2018). MAVEN observations of solar wind-driven magnetosonic waves heating the Martian dayside ionosphere. *Journal of Geophysical Research: Space Physics*, 123, 4129–4149. <https://doi.org/10.1029/2018JA025208>
- Frankland, V. L., James, A. D., Sánchez, J. D. C., Mangan, T. P., Willacy, K., Poppe, A. R., & Plane, J. M. C. (2016). Uptake of acetylene on cosmic dust and production of benzene in Titan's atmosphere. *Icarus*, 278, 88–99. <https://doi.org/10.1016/j.icarus.2016.06.007>
- Gerard, J.-C., Hubert, B., Ritter, B., Shematovich, V. I., & Bisikalo, D. V. (2018). Lyman- $\alpha$  emission in the Martian proton aurora: line profile and role of horizontal induced magnetic field. *Icarus*, 321, 266–271. <https://doi.org/10.1016/j.icarus.2018.11.013>
- Gombosi, T. I., Cravens, T. E., Nagy, A. F., Elphic, R. C., & Russell, C. T. (1980). Solar wind absorption by Venus. *Journal of Geophysical Research*, 85(A13), 7747–7753. <https://doi.org/10.1029/JA085iA13p07747>
- Grebowsky, J. M., Benna, M., Plane, J. M. C., Collinson, G. A., Mahaffy, P. R., & Jakosky, B. M. (2017). Unique, non-Earthlike, meteoritic ion behavior in upper atmosphere of Mars. *Geophysical Research Letters*, 44, 3066–3072. <https://doi.org/10.1002/2017GL072635>
- Gupta, S., & Upadhyaya, A. K. (2019). Morphology of Martian low-altitude ionospheric layer: MGS observations. *Journal of Geophysical Research: Space Physics*, 124, 2135–2151. <https://doi.org/10.1029/2018JA026162>
- Halekas, J. S., Ruhunusiri, S., Harada, Y., Collinson, G., Mitchell, D. L., Mazelle, C., et al. (2017). Structure, dynamics, and seasonal variability of the Mars-solar wind interaction: MAVEN Solar Wind Ion Analyzer in-flight performance and science results. *Journal of Geophysical Research: Space Physics*, 122, 547–578. <https://doi.org/10.1002/2016JA023167>
- Halekas, J. S., Taylor, E. R., Dalton, G., Johnson, G., Curtis, D. W., McFadden, J. P., et al. (2015). The Solar Wind Ion Analyzer for MAVEN. *Space Science Reviews*, 195(1-4), 125–151. <https://doi.org/10.1007/s11214-013-0029-z>
- Heavens, N. G., Kleinböhl, A., Chaffin, M. S., Halekas, J. S., Kass, D. M., Hayne, P. O., et al. (2018). Hydrogen escape from Mars enhanced by deep convection in dust storms. *Nature Astronomy*, 2(2), 126–132. <https://doi.org/10.1038/s41550-017-0353-4>
- Jakosky, B. M., Brain, D., Chaffin, M., Curry, S., Deighan, J., Grebowsky, J., et al. (2018). Loss of the Martian atmosphere to space: Present-day loss rates determined from MAVEN observations and integrated loss through time. *Icarus*, 315, 146–157. <https://doi.org/10.1016/j.icarus.2018.05.030>
- Jakosky, B. M., Slipski, M., Benna, M., Mahaffy, P., Elrod, M., Yelle, R., et al. (2017). Mars' atmospheric history derived from upper-atmosphere measurements of  $^{38}\text{Ar}/^{36}\text{Ar}$ . *Science*, 355(6332), 1408–1410. <https://doi.org/10.1126/science.aai7721>
- Kallio, E., & Barabash, S. (2001). Atmospheric effects of precipitating energetic hydrogen atoms on the Martian atmosphere. *Journal of Geophysical Research*, 106(A1), 165–177. <https://doi.org/10.1029/2000JA002003>
- Kislyakova, K. G., Holmstrom, M., Lammer, H., Odert, P., & Khodachenko, M. L. (2014). Magnetic moment and plasma environment of HD 209458b as determined from *Lya* observations. *Science*, 346(6212), 981–984. <https://doi.org/10.1126/science.1257829>
- Kliore, A. J., Nagy, A. F., Marouf, E. A., French, R. G., Flasar, F. M., Rappaport, N. J., et al. (2008). First results from the Cassini radio occultations of the Titan ionosphere. *Journal of Geophysical Research*, 113, A09317. <https://doi.org/10.1029/2007JA012965>
- Kopf, A. J., Gurnett, D. A., Morgan, D. D., & Kirchner, D. L. (2008). Transient layers in the topside ionosphere of Mars. *Geophysical Research Letters*, 35, L17102. <https://doi.org/10.1029/2008GL034948>
- Larson, D. E., Lillis, R. J., Lee, C. O., Dunn, P. A., Hatch, K., Robinson, M., et al. (2015). The MAVEN solar energetic particle investigation. *Space Science Reviews*, 195(1-4), 153–172. <https://doi.org/10.1007/s11214-015-0218-z>
- Lee, C. O., Hara, T., Halekas, J. S., Thiemann, E., Chamberlin, P., Eparvier, F., et al. (2017). MAVEN observations of the solar cycle 24 space weather conditions at Mars. *Journal of Geophysical Research: Space Physics*, 122, 2768–2794. <https://doi.org/10.1002/2016JA023495>
- Mendillo, M., & Evans, J. V. (1974). Incoherent scatter observations of the ionospheric response to a large solar flare. *Radio Science*, 9(2), 197–203. <https://doi.org/10.1029/RS009i002p00197>
- Mendillo, M., Narvaez, C., Vogt, M. F., Mayyasi, M., Forbes, J., Galand, M., et al. (2017). Sources of ionospheric variability at Mars. *Journal of Geophysical Research: Space Physics*, 122, 9670–9684. <https://doi.org/10.1002/2017JA024366>
- Mendillo, M., Narvaez, C., Vogt, M. F., Mayyasi, M., Mahaffy, P., Benna, M., et al. (2017). MAVEN and the total electron content of the Martian ionosphere. *Journal of Geophysical Research: Space Physics*, 122, 3526–3537. <https://doi.org/10.1002/2016JA023474>
- Pätzold, M., Tellmann, S., Häusler, B., Bird, M. K., Tyler, G. L., Christou, A. A., & Withers, P. (2009). A sporadic layer in the Venus lower ionosphere of meteoric origin. *Geophysical Research Letters*, 36, L21702. <https://doi.org/10.1029/2008GL035875>
- Pätzold, M., Tellmann, S., Häusler, B., Hinson, D., Schaa, R., & Tyler, G. L. (2005). A sporadic third layer in the ionosphere of Mars. *Science*, 310(5749), 837–839. <https://doi.org/10.1126/science.1117755>
- Peter, K. (2018). Small scale disturbances in the lower dayside ionosphere of Mars as seen by the MaRS radio science experiment on Mars Express., Diss. Universität zu Köln.
- Plane, J. M. C., Carrillo-Sanchez, J. D., Mangan, T. P., Crismani, M. M. J., Schneider, N. M., & Määttänen, A. (2018). Meteoric metal chemistry in the Martian atmosphere. *Journal of Geophysical Research: Planets*, 123, 695–707. <https://doi.org/10.1002/2017JE005510>
- Plane, J. M. C., Flynn, G. J., Määttänen, A., Moores, J. E., Poppe, A. R., Carrillo-Sanchez, J. D., & Listowski, C. (2018). Impacts of cosmic dust on planetary atmospheres and surfaces. *Space Science Reviews*, 214(1), 23.
- Ritter, B., Gérard, J.-C., Hubert, B., Rodriguez, L., & Montmessin, F. (2018). Observations of the proton aurora on Mars with SPICAM on board Mars Express. *Geophysical Research Letters*, 45, 612–619. <https://doi.org/10.1002/2017GL076235>
- Royer, E. M., Esposito, L. W., Crary, F., & Wahlund, J. E. (2018). Enhanced airglow signature observed at Titan in response to its fluctuating magnetospheric environment. *Geophysical Research Letters*, 45, 8864–8870. <https://doi.org/10.1029/2018GL078870>
- Schneider, N. M., Jain, S. K., Deighan, J., Nasr, C. R., Brain, D. A., Larson, D., et al. (2018). Global aurora on Mars during the September 2017 Space Weather event. *Geophysical Research Letters*, 45, 7391–7398. <https://doi.org/10.1029/2018GL077772>
- Schneider, N. M., Deighan, J. I., Jain, S. K., Stiepen, A., Stewart, A. I. F., Larson, D., et al. (2015). Discovery of diffuse aurora on Mars. *Science*, 350(6261), aad0313. <https://doi.org/10.1126/science.aad0313>

- Schneider, N. M., Deighan, J. I., Stewart, A. I. F., McClintock, W. E., Jain, S. K., Chaffin, M. S., et al. (2015). MAVEN IUVS observations of the aftermath of the Comet Siding Spring meteor shower on Mars. *Geophysical Research Letters*, *42*, 4755–4761. <https://doi.org/10.1002/2015GL063863>
- Schwartz, S. J., & Burgess, D. (1991). Quasi-parallel shocks: A patchwork of three-dimensional structures. *Geophysical Research Letters*, *18*(3), 373–376. <https://doi.org/10.1029/91GL00138>
- Thomsen, M. F., Gosling, J. T., Bame, S. J., & Russell, C. T. (1990). Magnetic pulsations at the quasi-parallel shock. *Journal of Geophysical Research*, *95*(A2), 957–966. <https://doi.org/10.1029/JA095iA02p00957>
- Withers, P. (2009). A review of observed variability in the dayside ionosphere of Mars. *Advances in Space Research*, *44*(3), 277–307. <https://doi.org/10.1016/j.asr.2009.04.027>
- Withers, P., Felici, M., Mendillo, M., Moore, L., Narvaez, C., Vogt, M. F., & Jakosky, B. M. (2018). First ionospheric results from the MAVEN Radio Occultation Science Experiment (ROSE). *Journal of Geophysical Research: Space Physics*, *123*, 4171–4180. <https://doi.org/10.1029/2018JA025182>
- Withers, P., Fillingim, M. O., Lillis, R. J., Häusler, B., Hinson, D. P., Tyler, G. L., et al. (2012). Observations of the nightside ionosphere of Mars by the Mars Express radio science experiment (MaRS). *Journal of Geophysical Research*, *117*, A12307. <https://doi.org/10.1029/2012JA018185>
- Withers, P., Mendillo, M., Hinson, D. P., & Cahoy, K. (2008). Physical characteristics and occurrence rates of meteoric plasma layers detected in the Martian ionosphere by the Mars Global Surveyor Radio Science Experiment. *Journal of Geophysical Research*, *113*, A12314. <https://doi.org/10.1029/2008JA013636>
- Zhang, T. L., du, J., Ma, Y. J., Lammer, H., Baumjohann, W., Wang, C., & Russell, C. T. (2009). Disappearing induced magnetosphere at Venus: Implications for close-in exoplanets. *Geophysical Research Letters*, *36*, L20203. <https://doi.org/10.1029/2009GL040515>